OXFORD

Cerebral Cortex, 2015, 1–13

doi: 10.1093/cercor/bhv026
Original Article

ORIGINAL ARTICLE

Altered Structural Brain Networks in Tuberous Sclerosis Complex

Kiho Im[1,2], Banu Ahtam[1,2], Daniel Haehn[2,3], Jurriaan M. Peters[4,5], Simon K. Warfield[3,5], Mustafa Sahin[4], and P. Ellen Grant[1,2,3,6]

[1]Division of Newborn Medicine, [2]Fetal Neonatal Neuroimaging and Developmental Science Center, [3]Department of Radiology, [4]Department of Neurology, [5]Computational Radiology Laboratory, Boston Children's Hospital, Harvard Medical School, Boston, MA 02115, USA, and [6]Department of Radiology, Massachusetts General Hospital, Athinoula A. Martinos Center for Biomedical Imaging, Charlestown, MA 02119, USA

Address correspondence to Kiho Im, Boston Children's Hospital, 1 Autumn Street, Boston, MA 02115, USA. Email: kiho.im@childrens.harvard.edu

Kiho Im and Banu Ahtam contributed equally to this study.

Abstract

Tuberous sclerosis complex (TSC) is characterized by benign hamartomas in multiple organs including the brain and its clinical phenotypes may be associated with abnormal neural connections. We aimed to provide the first detailed findings on disrupted structural brain networks in TSC patients. Structural whole-brain connectivity maps were constructed using structural and diffusion MRI in 20 TSC (age range: 3–24 years) and 20 typically developing (TD; 3–23 years) subjects. We assessed global (short- and long-association and interhemispheric fibers) and regional white matter connectivity, and performed graph theoretical analysis using gyral pattern- and atlas-based node parcellations. Significantly higher mean diffusivity (MD) was shown in TSC patients than in TD controls throughout the whole brain and positively correlated with tuber load severity. A significant increase in MD was mainly influenced by an increase in radial diffusivity. Furthermore, interhemispheric connectivity was particularly reduced in TSC, which leads to increased network segregation within hemispheres. TSC patients with developmental delay (DD) showed significantly higher MD than those without DD primarily in intrahemispheric connections. Our analysis allows non-biased determination of differential white matter involvement, which may provide better measures of "lesion load" and lead to a better understanding of disease mechanisms.

Key words: brain networks, developmental delay, diffusion tensor imaging, structural connectivity, tuberous sclerosis complex

Introduction

Tuberous sclerosis complex (TSC) is an autosomal dominant disorder caused primarily by mutations in *TSC1* or *TSC2* genes, and characterized by benign hamartomatous lesions in multiple organs including the brain (Baskin 2008). The clinical phenotype is widely variable, but the majority of TSC patients show neurological manifestations of the disorder including seizures (90%), developmental delay (DD) or intellectual disability (50%), neurobehavioral abnormalities, and autism spectrum disorders (ASDs, 50%; Baskin 2008; Curatolo et al. 2008). Mouse model studies have found that mutations in *Tsc1* or *Tsc2* genes cause abnormal neuronal connections. *Tsc1*-deleted mice are shown to display seizures and have delayed myelination (Meikle et al. 2007). *Tsc2* heterozygous mice show aberrant topographic projections of axon pathways in the reticulogeniculate tract (Nie et al. 2010). Thus, there is evidence from mouse models of aberrant connectivity in TSC.

Although cortical tubers are one of the hallmarks of TSC (Curatolo et al. 2002), there is no consistent correlation between the number and location of tubers, and epileptic seizures (Major et al. 2009) or autistic features (Bolton et al. 2002; Numis et al. 2011). Therefore, it has been suggested that the broad spectrum

of TSC clinical phenotypes may arise from abnormal neural connections that are independent of these benign tumors (Tsai and Sahin 2011; Peters, Taquet, Vega, et al. 2013). Human diffusion tensor imaging (DTI) studies have reported decreased fractional anisotropy (FA) and increased mean diffusivity (MD) values in certain brain structures such as the corpus callosum, internal capsule, and external capsule in patients with TSC compared with typically developing (TD) individuals (Makki et al. 2007; Krishnan et al. 2010; Peters et al. 2012). However, although selective tracts have been analyzed, unbiased whole-brain connectivity measures have not been performed.

To assess whole-brain white matter connectivity in an unbiased manner, a human brain connectome approach can be used. This approach models the complex network of brain connectivity with a graph using a set of nodes and interconnecting edges to provide measures of whole-brain structural connectivity (Sporns et al. 2005). To define the nodes, most studies parcellated cortical regions using volume- or surface-based registration to an atlas (Tzourio-Mazoyer et al. 2002; Desikan et al. 2006). However, the use of atlas-based parcellation techniques causes many short intergyral connections to be ignored and heterogeneously connected brain regions to be lumped into single nodes. To overcome these limitations, we used a gyral topology-based parcellation scheme, which we believe is a more appropriate node definition method for the description of the whole-brain white matter network (Im et al. 2014).

The aim of this study was to perform a non-biased whole-brain analysis of global white matter connectivity (short- and long-association and interhemispheric fiber connections) using gyral pattern-based cortical node parcellations and regional connectivity using atlas-based parcellations. We also performed graph theoretical global network analysis using both gyral and atlas-based approaches, and compared their results. In TSC patients, all connectivity and network measurements were compared between subgroups defined by the presence of an ASD, epilepsy, and DD, as well as tuber load.

Materials and Methods

Participants

Twenty patients (age range, 3–24 years; 11 males and 9 females) with a diagnosis of TSC and 20 age- and gender-matched TD participants (age range, 2–23 years; 7 males and 13 females) were imaged using a 3-T MRI. All TSC patients had a neurological examination, and their clinical data were obtained through their office visits and medical records. All patients fulfilled the clinical criteria for a definite TSC diagnosis, as defined by the Tuberous Sclerosis Consensus Conference. ASD diagnoses were made by a board-certified pediatric neurologist based on the Diagnostic and Statistical Manual of Mental Disorders, Fourth Edition, Text Revision (APA 2000) as well as the Autism Diagnostic Observation Schedule (Lord et al. 2000), administered by trained behavioral specialists. All available clinical, research, and neuropsychological data were reviewed on a case-by-case basis by a pediatric neurologist to identify those with moderate to severe DD. Of the 20 TSC participants, 7 were diagnosed with an ASD, 9 with epilepsy, and 11 with DD. Eleven TSC patients had the *TSC2* gene involved in their diagnosis as either deletion, insertion, or mutation. Four TSC patients were diagnosed both with ASD and DD; 1 TSC patient was diagnosed with ASD and epilepsy; 4 TSC patients were diagnosed with epilepsy and DD; and 2 TSC patients were diagnosed with ASD, epilepsy, and DD. None of the TSC participants had undergone prior surgery. The "tuber load" was visually assessed using fluid-attenuated inversion recovery (FLAIR) images separately by 2 independent readers, a certified neuroradiologist and a certified neurologist (P.E.G. and J.M.P.). The reviewers qualitatively placed TSC brains into 1 of 4 different groups, defined by tuber volume relative to whole-brain volume, such as 1. minimal: <1/8 of the brain volume, 2. mild: >1/8 but <1/4 of the brain volume, 3. moderate: >1/4 but <1/2 of the brain volume, and 4. severe: >1/2 of the brain volume. After the initial independent review, a consensus was reached between the 2 physicians on the 4 cases who differed by only one grade. Demographic and clinical data for all TSC patients are presented in Table 1. The 20 TSC patients are a subgroup of the TSC patients whose data were analyzed by Peters et al. (2012) where only corpus callosum connectivity was assessed. The TD control participants were chosen from individuals who were clinically normal apart from symptoms of headache who underwent MRI examinations as a screening precaution; control datasets were chosen from those individuals who had normal brain MRI examinations as determined by 2 pediatric neuroradiologists and no clinical diagnosis associated with cerebral disorders including migraine. This study was approved by the institutional review board of Boston Children's Hospital.

MRI Acquisition

The imaging protocol consisted of a structural and diffusion-weighted sequence. The structural sequence was a T_1-weighted high-resolution magnetization-prepared rapid-acquisition gradient-echo (MPRAGE) acquisition (voxel size [mm] = 0.5 × 0.5 × 1–1 × 1 × 1; field of view [FOV] = 19.2–25.6 cm; echo time [TE] = 1.66–3.39 ms; repetition time [TR] = 1130–2530 ms; flip angle = 7–9°). The diffusion sequence was an axial echo-planar sequence (voxel size [mm] = 1.7 × 1.7 × 2.2; FOV = 22 cm; TE = 88 ms; TR = 1000 ms; flip angle = 90°; in-plane GRAPPA acceleration factor = 2, number of averages acquired = 1; 30 gradient diffusion directions at $b = 1000$ s/mm^2; 5 acquisitions with $b = 0$ s/mm^2). Sedation, typically dexmedetomidine, was used only when necessary (e.g., very young children, intellectual impairment, and behavioral difficulties), to prevent excessive motion. Dexmedetomidine has been proved to be a safe and effective sedation technique, producing a condition similar to natural sleep (Mason 2010) for MRI (Siddappa et al. 2011; Ambi et al. 2012), and is the suggested sedation technique that is commonly used for children with neurobehavioral disorders such as autism (Lubisch et al. 2009). As there is only minor perturbation of neuronal activity with dexmedetomidine, diffusion metrics such as FA and MD, which are modulated by water compartmentalization, are unlikely to show any significant change. Currently, there are no reports of diffusion metric changes related to sedation administration.

To assess the degree of motion artifacts in each individual and test if the TSC patients showed a larger head motion, we performed a quantitative motion estimation analysis. All diffusion images in the series were aligned to the first b_0 image using affine registration (Jenkinson et al. 2002). Average volume-by-volume translation and rotation were extracted from affine transformation of the diffusion volumes, and a single value, "total motion index" (TMI), was calculated (Yendiki et al. 2013). The TMI values were statistically compared between the TSC and TD groups with an independent sample *t*-test.

Image Processing: Cortical Surface Reconstruction and White Matter Tractography

Data were processed with the Connectome Mapper (CMP; Daducci et al. 2012; http://www.cmtk.org/mapper), which includes the use

Table 1 Demographic and clinical data for individual TSC patients

ID	Gender	Age (years)	ASD	Epilepsy	Developmental delay	Genetics	Clinical summary	Tuber load
1	M	3.21	No	Yes	Yes	TSC2 del,*	H, F, O	Minimal
2	F	3.9	No	No	No	TSC1 mut,**,#	H	Minimal
3	M	3.97	No	Yes	Yes	TSC2 del,*	C, H, F, O, R	Severe
4	M	5.06	No	No	No	TSC1 & 2 N,***	C, R	Minimal
5	M	5.8	Yes	Yes	Yes	TSC1 & 2 N, unk.	H	Moderate
6	M	6.49	Yes	No	Yes	TSC2 mut,**	C, H, F, R, I	Moderate
7	F	6.81	No	Yes	No	TSC1 mut,#	C, H	Minimal
8	M	7.5	No	No	No	TSC2 ins,#	H, F, R	Minimal
9	M	7.55	No	No	No	n/a	H, F, O, R	Mild
10	M	7.57	Yes	Yes	No	TSC2 mut,**	H, F	Minimal
11	F	8.47	No	Yes	No	TSC1 & 2 N	C, H, F, R	Mild
12	F	9.24	No	Yes	Yes	TSC2 del,*	H	Mild
13	M	10.67	No	Yes	Yes	TSC2 mut,*	C, H, F, O	Mild
14	M	13.9	Yes	No	Yes	TSC2 mut,*	C, H, F, O, R, I	Moderate
15	F	16.07	No	No	No	TSC2 mut,**, unk.	F, O, R	Minimal
16	F	17.49	No	No	Yes	TSC2 del,*	H, F, R, I	Minimal
17	M	21.96	No	No	No	TSC1 & 2 N	F, R	Minimal
18	F	21.97	Yes	Yes	Yes	TSC2 ins,***	R	Mild
19	F	24.06	Yes	No	Yes	n/a	C, F, R, I	Moderate
20	F	24.88	Yes	No	Yes	TSC2 mut,*	H, F, O, R, I	Severe

M: male; F: female; Genetics—N: normal; *: de novo mutation; **: unknown variant, likely pathogenic; ***: known parental mutation or family history of TSC; #: parental testing unknown; unk.: unknown; n/a: not available; Del: deletion; Ins: insertion; mut: mutation; Clinical summary—C: cardiac rhabdomyomas; H: hypomelanotic macules; F: facial angiofibroma; O: other neurocutaneous (ash leaf, shagreen patch, confetti lesions, forehead plaque, periungual fibroma, and retinal abnormalities); R: renal angiomyolipomas; I: infantile spasms (with later epilepsy).

of several neuroimaging tools such as FSL (http://www.fmrib.ox.ac.uk/fsl), FreeSurfer (http://surfer.nmr.mgh.harvard.edu), and Diffusion Toolkit (http://www.trackvis.org/dtk).

First, T_1-weighted images were processed to extract cortical surfaces using FreeSurfer (Dale et al. 1999; Fischl et al. 1999). FSL's intensity-based affine registration tool, FLIRT, was used to register the structural T_1-weighted image onto the diffusion space, namely to the b_0 image. CMP uses the Diffusion Toolkit for intravoxel configuration of fibers. Whole-brain tractography was performed with a DTI model and a streamline algorithm that accounts for diffusion directions in a voxel. Fiber tracking was constrained inside the white matter with the use of a high-resolution binary mask for the white matter, which was computed by FreeSurfer. Angle threshold was set to 85° and seed parameter was set to 32 in order to enable the start of multiple trajectories for every direction inside each voxel. A fiber cutoff filter was applied so that fibers shorter than 20 mm and longer than 200 mm were filtered. For more reliable callosal fiber tracts, the corpus callosum was detected with the use of structural MRI scans and standard DTI color-coded FA maps. A three-dimensional corpus callosum region of interest (ROI) was manually segmented for each dataset in TrackVis (http://www.trackvis.org) using previously established criteria (Catani and Thiebaut de Schotten 2008). The few spurious connections (e.g., fibers that start and end in the same hemisphere after crossing to the other hemisphere) were manually removed using TrackVis.

Tuber Load and Whole-Brain Fiber Count Analyses

To test if our findings for white matter connectivity in TSC are biased by poor tracking in areas of cortical tubers in this patient population, we first investigated fiber tracking in the whole brain by comparing the number of fiber tracts according to different groups (TD vs. TSC) and tuber load severity within the TSC group.

Structural Connectivity Network Construction

Network Node Definition

To define the nodes of a brain graph, we first obtained 68 cortical regions using the automatic cortical parcellation provided by FreeSurfer (Fischl et al. 2004; Desikan et al. 2006). We also performed an individual gyral pattern-based parcellation for node definition. To create the gyral-based parcellation, we used a sulcal depth map measured on the white matter surface to parcellate gyral segments (Fischl et al. 1999). We then performed a watershed algorithm based on the depth map on triangular meshes (Im et al. 2010, 2011, 2013). To prevent over-extraction of the gyral segments, we first reduced noisy depth variations with a surface-based heat kernel smoothing with a full-width half-maximum value of 10 mm (Chung et al. 2005). Subsequently, we performed segment merging in the watershed algorithm using the area of the segment. If one of the areas of 2 or more gyral segments was smaller than a threshold (30 mm^2) when they met at a ridge point, the smaller region below the threshold was merged into the adjacent gyral region. The result of the gyral-based parcellation is shown and can be compared to the atlas-based anatomical parcellation using FreeSurfer in Figure 1. The gyral pattern-based parcellation method divided the cortical surface into more regions than FreeSurfer. The average number and area of gyral nodes in the whole brain was 161.3 (range: 152–172) and 9.32 cm^2 (standard deviation [SD]: 5.90 cm^2) for TD individuals, and 163.2 (143–177) and 8.92 cm^2 (SD: 5.83 cm^2) for the TSC patients. FreeSurfer parcellation defined fewer regions (68) and variably segmented the brain into gyral segments, gyri, or multiple gyri. Average and SD of the area of FreeSurfer parcellation nodes were 21.68 and 17.15 cm^2 for TD, and 21.08 and 17.04 cm^2 for TSC. Gyral-based segmentation provided a more uniform and consistent segmentation with regions that are similar in size and with equal respect for gyral topology (Fig. 1).

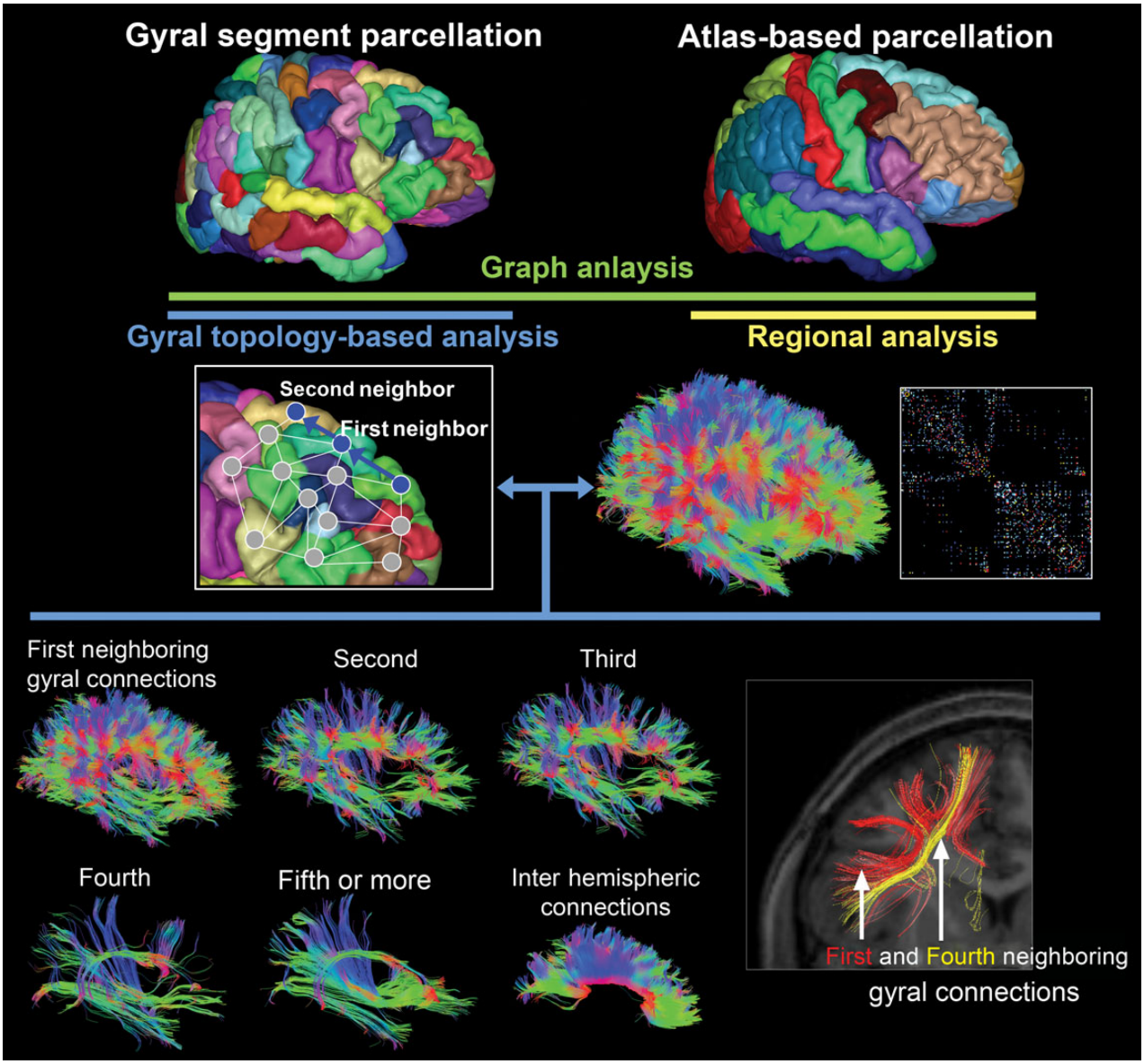

Figure 1. Atlas-based parcellation using FreeSurfer and individual gyral pattern-based parcellation. The gyral node parcellation was used for short- and long range, and interhemispheric white matter connectivity as well as graph theoretical network analyses. The atlas-based parcellation was used for regional connectivity as well as graph theoretical analyses.

Network Edge Definition

T_1-weighted images were coregistered to the diffusion images as described above. Two nodes (regions) were considered to have a structural connection (edge), when at least the end points of 2 fiber tracts were located <3 mm from each of the 2 surface node regions, with self-connections excluded (Im et al. 2014). A threshold of the number of fiber tracts was selected to reduce the risk of false-positive connections due to noise or the limitations in the deterministic tractography (Lo et al. 2010; Shu et al. 2011). The number of fiber tracts performed with streamline tracking may reflect the structure of the white matter (Houenou et al. 2007), and has been used to calculate the weight of network edges (Shu et al. 2011; Yan et al. 2011; Zhang et al. 2011; Batalle et al. 2012), but it largely depends on the brain size (the number of white matter voxels) and the areas of node regions. For each edge, the "connection density" (the number of fiber tracts per unit surface) was calculated between 2 nodes, N_{ij}/S_{ij}, where N_{ij} is the number of tracts between region i and j, and S_{ij} is the surface area of 2 regions, i and j. We also measured the mean values of FA, MD, radial diffusivity (RD), and axial diffusivity (AD) along all the fibers connecting a pair of cortical regions.

Analysis for Gyral Topology-Based Node Definition

We constructed and analyzed different fiber groups and networks subdivided according to the individual gyral pattern-based node definition. If 2 gyral segments geometrically met on the cortical surface, they were connected with an edge and became first neighbors to each other. We then defined the first, second, third, fourth, and fifth or more neighbors for each gyral region by measuring the number of edges in the shortest paths (Fig. 1). The connections between the first neighboring gyri were taken to be short association U-fiber connections, and the connections between distant gyri were taken to be long-

association fiber connections (Fig. 1). We separately measured the mean FA, MD, RD, and AD as well as a basic network measure, "network density," for the connections between the *n*th neighboring gyri and between the hemispheres. The network density was measured as the fraction of present connections to possible connections between the *n*th neighboring gyri without considering the connection weights.

Graph Theoretical Global Network Analysis

Graph theoretical analyses were carried out on weighted connectivity networks of patients with TSC and TD individuals using the Brain Connectivity Toolbox (http://www.brain-connectivity-toolbox.net; Rubinov and Sporns 2010). Graph measures were computed for both the networks derived from the FreeSurfer parcellation nodes and the individual gyral pattern-based nodes. For the network analysis conducted in this study, we weighted the edge connecting 2 nodes with the connection density and also used MD and FA to modify strengths of interregional connections because they are important markers for evaluating fiber integrity and white matter development and maturation (myelin and axonal diameter changes) (Beaulieu 2002; Hagmann et al. 2010). We used the product between the connection density and mean inverse MD (1/MD) (Hagmann et al. 2008, 2010). The value resulting from multiplying the connection density by the mean FA was also used for another edge weight.

We calculated the weighted "clustering coefficient" and "transitivity" as measures of network segregation (Onnela et al. 2005). To measure network integration, we calculated the average shortest path length between all pairs of nodes in the network, which is known as the "characteristic path length" of the network (Watts and Strogatz 1998). In addition, the "global efficiency" was computed as the average inverse shortest path length (Latora and Marchiori 2001). The graph measures were scaled against the mean values of graph measures obtained from 1000 matched random graphs that preserved the same number of nodes, edges, and degree sequence (Maslov and Sneppen 2002).

Regional Network Analysis

Following the analysis of the global network organization, we further localized specific connections and regions in which the structural connectivity was impaired in patients. Gyral parcellation nodes were not used for regional analysis because the number of nodes was not constant and node correspondence was not defined. We compared the values of FA, MD, RD, and AD between the TD and TSC groups for each connection between 2 regions in the network of the FreeSurfer parcellation nodes. However, identification of edges between nodes was not identical across participants. Hence, pairs of regions where edges were identified in >80% of TD and TSC participants were statistically analyzed.

Statistical Analysis

Group differences in the fiber tract number, global and regional connectivity, and network measures were statistically assessed between the TD and TSC groups using multiple linear regression analysis. The dependent variable (Y) was each measurement, and the independent variable was group (coded as a dummy variable). We also used age as a covariate to control for its effect (model fit: $Y = b_0 + b_1\text{group} + b_2\text{age}$). The assumptions of linearity, independence of errors, homoscedasticity, unusual points, and normality of residuals were met for each of the models.

To compare 2 small subgroups divided by the presence of ASD, epilepsy, and DD in TSC patients, first, age was regressed out as a covariate. Then, the Mann–Whitney *U*-test was performed, which is a non-parametric statistical test for the comparison of independent 2 samples. To determine any significant relationship between tuber load score (minimum = 1, mild = 2, moderate = 3, and severe = 4) and white matter connectivity, Spearman's correlation coefficients were calculated, where we controlled for age adding it as a covariate.

Gyral topology-based connectivity analysis was performed for the 5 gyral and corpus callosum connections. The statistics were set to a significance threshold of $P = 0.008$ (0.05/6) to control for multiple comparisons with Bonferroni correction. For the edge-based regional analysis, false discovery rate control was used for adjusting statistical results for multiple group comparisons (Genovese et al. 2002). Gyral node-based connectivity networks had a different number of nodes across participants. Comparisons of graph measures are influenced by the number of nodes of the network (van Wijk et al. 2010; Zalesky et al. 2010). We statistically controlled for the remaining effect of the number of nodes by adding it as a covariate when we compared gyral node-based network measures between groups (network density, clustering coefficient, transitivity, characteristic path length, and global efficiency; Im et al. 2014).

Results

Head Motion Analysis

All 40 cases had good quality structural and diffusion MRI data clean of artifacts. For the TMI values estimated from DTI, there was no significant difference between TD controls (TMI [mean ± SD]: 0.368 ± 0.956) and TSC patients (0.534 ± 1.810) ($P = 0.723$).

Fiber Tracking and the Number of Fiber Tracts in TSC

The results of the multiple linear regression analysis showed that the number of fibers in the whole brain did not significantly differ between the TD (19 393.30 ± 5409.22) and TSC (18 542.40 ± 4297.01) groups ($P = 0.441$).

There was not any significant relationship between the qualitative assessment of tuber load and the number of fibers in the whole brain in TSC patients according to the Spearman's correlation coefficient results (correlation coefficient $r = -0.345$, $P = 0.148$).

To further illustrate our findings, we manually created two 3D ROIs covering the volume of a cortical tuber and a region of white matter abnormality in a TSC patient, using the axial FLAIR image. We also placed the same ROIs on a TD participant's brain in the same locations. We extracted the fiber tracts that passed only through these ROIs in both participants. The results of our tuber ROI analysis showed that even though the number of fibers passing through the ROIs in both the TD and the TSC participant was very similar, the diffusivity values of FA, MD, AD, and RD showed differences between the 2 participants (see Supplementary Fig. 1).

Global Characteristics of Connectivity Networks

Gyral node-based graph analysis revealed a significantly higher clustering coefficient in TSC compared with TD for both edge weights (connection density × 1/MD: $P = 0.043$, connection density × FA: $P = 0.046$). No significant difference was found in transitivity, characteristic path length, and global efficiency. Global network analysis using the FreeSurfer parcellation did not

Table 2 Statistical results for the group comparisons of graph measures based on gyral parcellation nodes and FreeSurfer parcellation nodes

Connection weight	Measure	TD	TSC	P-value
Gyral parcellation				
Connection density × 1/MD	Clustering coefficient	5.993 ± 0.498	6.346 ± 0.575	0.043*
	Transitivity	4.362 ± 0.507	4.519 ± 0.460	0.318
	Characteristic path length	1.383 ± 0.100	1.352 ± 0.114	0.367
	Global efficiency	0.795 ± 0.036	0.803 ± 0.049	0.496
Connection density × FA	Clustering coefficient	5.815 ± 0.516	6.174 ± 0.630	0.046*
	Transitivity	4.389 ± 0.515	4.550 ± 0.487	0.314
	Characteristic path length	1.347 ± 0.106	1.310 ± 0.107	0.294
	Global efficiency	0.821 ± 0.039	0.833 ± 0.052	0.417
FreeSurfer parcellation				
Connection density × 1/MD	Clustering coefficient	3.266 ± 0.322	3.376 ± 0.362	0.248
	Transitivity	2.463 ± 0.216	2.509 ± 0.283	0.504
	Characteristic path length	1.189 ± 0.105	1.190 ± 0.075	0.965
	Global efficiency	0.886 ± 0.044	0.877 ± 0.029	0.470
Connection density × FA	Clustering coefficient	3.181 ± 0.312	3.272 ± 0.329	0.296
	Transitivity	2.493 ± 0.220	2.537 ± 0.293	0.526
	Characteristic path length	1.223 ± 0.097	1.208 ± 0.070	0.597
	Global efficiency	0.897 ± 0.044	0.898 ± 0.031	0.866

Note: data are denoted as mean ± SD.
*$P < 0.05$.

show statistical significance for any of the graph measures. Statistical results for the group comparisons are presented in Table 2. Within the TSC patients, there was no statistically significant difference between the subgroups in any of the global graph measures.

Structural Connectivity Based on Gyral Topological Path Length in the Whole Brain

For the group analysis between TSC and TD, the statistics (mean, SD, and *P*-values) are listed in Table 3. Mean FA was lower in the TSC group than the TD group in all of the gyral connections and in the corpus callosum, but the difference did not reach significance after multiple comparisons correction. MD was significantly higher in TSC than TD ($P < 0.008$) for the second, third, and fourth gyral neighbor connections as well as the corpus callosum, but not for the first and fifth or more gyral neighbor connections. RD was significantly increased in the TSC group for all the connections ($P < 0.008$), except for the fifth or more gyral neighbor connection. Mean AD was higher in TSC than TD for all the connections, but this result was not significant at $P = 0.008$. The difference of network density between the groups was not statistically significant for any of the gyral neighbor connections and the corpus callosum after multiple comparisons correction.

In the TSC subgroup comparisons, TSC patients with DD had significantly increased MD values than those without DD for all the gyral neighbor connections ($P < 0.008$), but not for corpus callosum (Table 4). AD values were also significantly higher in TSC patients with DD compared with those without DD for almost all of the gyral neighbor connections but not for corpus callosum. RD values were significantly higher in TSC patients with DD than those without DD in first–fourth gyral neighbor connections. TSC patients with ASD had higher MD (second–fifth or more) and RD (third and fourth) values for the several gyral neighbor connections than those without ASD, but these results were not significant after multiple comparisons correction ($0.008 < P < 0.05$; see Supplementary Table 1). TSC patients with epilepsy did not have significantly different connectivity values compared with those without epilepsy (see Supplementary Table 2). Spearman's correlation analyses revealed a significant positive correlation between qualitative tuber load and MD as well as AD values of all the gyral neighbor connections and corpus callosum in the TSC patients ($P < 0.008$). Qualitative tuber load was also significantly correlated with RD values of first–fourth gyral neighbor connections ($P < 0.008$; Table 5).

Regional Characteristics of Connectivity Networks Using the Atlas-Based Parcellation

To better understand regional characteristics, atlas-based nodes were used as they correspond to predefined functional regions. Atlas-based regional connectivity analysis revealed significantly lower FA in 5 connections in the left temporal and right parietal regions in TSC compared with TD at the 0.05 level of FDR-corrected *P* (Fig. 2). TSC patients had significantly higher MD in 66 connections throughout the whole brain (Fig. 2). When we examined RD and AD separately, RD was also significantly higher in most of connections (44 connections) that were identified in the MD analysis, but AD was statistically significant only for 1 connection in the left temporal region (Fig. 2). The number of statistically significant edges was counted for each cortical node regions and mapped with a different node size on the figures. Right inferior parietal gyrus and its neighboring regions such as right superior parietal or supramarginal gyrus had the largest number of disrupted connections with other regions for FA, MD, and RD (Fig. 2). In the left hemisphere, inferior parietal gyrus had the largest number of connections showing significantly increased MD and RD (Fig. 2).

In the subgroup analysis, TSC patients with DD showed significantly higher MD in 56 connections in global brain regions than those with no DD (corrected $P < 0.05$; Fig. 3). RD and AD were also significantly greater in 6 connections and 16 connections, respectively, in TSC patients with DD compared with TSC patients without DD. Particularly, many connections from the right inferior parietal gyrus showed significant changes in MD and AD (Fig. 3). Local edge analysis in the TSC group revealed positive correlations between tuber load and MD (91 connections), RD (53 connections), and AD (84 connections) values

Table 3 Statistical results for the group comparisons of gyral connectivity and corpus callosum connectivity between TD and TSC groups

	First	Second	Third	Fourth	Fifth or more	Corpus callosum
FA						
TD	0.3697 ± 0.0211	0.3974 ± 0.0207	0.4189 ± 0.0226	0.4344 ± 0.0237	0.4442 ± 0.0313	0.5269 ± 0.0178
TSC	0.3530 ± 0.0273	0.3812 ± 0.0288	0.4011 ± 0.0300	0.4161 ± 0.0339	0.4331 ± 0.0373	0.5061 ± 0.0327
P-value	0.021	0.021	0.016	0.032	0.205	0.018
MD ($\times 10^{-4}$)						
TD	8.00 ± 0.41	8.04 ± 0.43	8.06 ± 0.46	8.12 ± 0.48	8.25 ± 0.49	8.23 ± 0.39
TSC	8.25 ± 0.42	8.39 ± 0.49	8.45 ± 0.50	8.57 ± 0.59	8.64 ± 0.63	8.62 ± 0.43
P-value	0.014	0.004*	0.002*	0.003*	0.009	0.001*
AD ($\times 10^{-4}$)						
TD	11.32 ± 0.46	11.71 ± 0.46	11.98 ± 0.49	12.27 ± 0.50	12.58 ± 0.55	13.79 ± 0.54
TSC	11.50 ± 0.55	12.02 ± 0.60	12.36 ± 0.59	12.71 ± 0.69	13.03 ± 0.75	14.07 ± 0.62
P-value	0.147	0.027	0.013	0.010	0.017	0.039
RD ($\times 10^{-4}$)						
TD	6.34 ± 0.41	6.21 ± 0.42	6.10 ± 0.46	6.05 ± 0.48	6.08 ± 0.51	5.46 ± 0.34
TSC	6.62 ± 0.40	6.57 ± 0.49	6.50 ± 0.51	6.50 ± 0.61	6.45 ± 0.66	5.89 ± 0.47
P-value	0.005*	0.003*	0.002*	0.004*	0.018	0.001*
Network density						
TD	0.7058 ± 0.0730	0.2407 ± 0.0359	0.1065 ± 0.0213	0.0551 ± 0.0161	0.0162 ± 0.0086	0.0158 ± 0.0040
TSC	0.7170 ± 0.0401	0.2468 ± 0.0237	0.1088 ± 0.0201	0.0585 ± 0.0149	0.0171 ± 0.0056	0.0128 ± 0.0041
P-value	0.789	0.759	0.932	0.696	0.933	0.034

Note: data are denoted as mean ± SD.
*$P < 0.008$.

Table 4 Statistical results for the group comparisons of gyral connectivity and corpus callosum connectivity between the TSC patients with DD (DD+) and the patients without DD (DD−)

	First	Second	Third	Fourth	Fifth or more	Corpus callosum
FA						
DD+	0.3485 ± 0.0305	0.3734 ± 0.0323	0.3927 ± 0.0335	0.4058 ± 0.0393	0.4293 ± 0.0464	0.4958 ± 0.0389
DD−	0.3585 ± 0.0235	0.3907 ± 0.0219	0.4115 ± 0.0227	0.4288 ± 0.0217	0.4377 ± 0.0240	0.5188 ± 0.0181
P-value	0.447	0.129	0.172	0.197	0.761	0.129
MD ($\times 10^{-4}$)						
DD+	8.44 ± 0.41	8.63 ± 0.47	8.70 ± 0.45	8.88 ± 0.57	8.92 ± 0.66	8.79 ± 0.44
DD−	8.01 ± 0.29	8.09 ± 0.33	8.14 ± 0.38	8.19 ± 0.37	8.31 ± 0.43	8.41 ± 0.34
P-value	0.002*	0.001*	0.001*	0.004*	0.004*	0.015
AD ($\times 10^{-4}$)						
DD+	11.73 ± 0.60	12.29 ± 0.62	12.64 ± 0.57	13.06 ± 0.67	13.39 ± 0.76	14.21 ± 0.69
DD−	11.22 ± 0.32	11.70 ± 0.39	12.01 ± 0.43	12.29 ± 0.55	12.59 ± 0.46	13.90 ± 0.49
P-value	0.005*	0.010	0.006*	0.005*	0.005*	0.068
RD ($\times 10^{-4}$)						
DD+	6.79 ± 0.40	6.80 ± 0.48	6.74 ± 0.48	6.79 ± 0.62	6.67 ± 0.74	6.08 ± 0.50
DD−	6.41 ± 0.31	6.29 ± 0.34	6.20 ± 0.38	6.14 ± 0.37	6.17 ± 0.44	5.67 ± 0.32
P-value	0.003*	0.002*	0.002*	0.003*	0.033	0.040
Network density						
DD+	0.7050 ± 0.0391	0.2368 ± 0.0207	0.1015 ± 0.0184	0.0537 ± 0.0121	0.0152 ± 0.0040	0.0114 ± 0.0031
DD−	0.7317 ± 0.0384	0.2590 ± 0.0222	0.1176 ± 0.0195	0.0644 ± 0.0166	0.0195 ± 0.0067	0.0146 ± 0.0047
P-value	0.095	0.048	0.028	0.081	0.172	0.224

Note: data are denoted as mean ± SD.
*$P < 0.008$.

throughout the whole brain at the 0.05 level of FDR-corrected *P*. Most of the connections with significant correlations between qualitative tuber load and the diffusivity values were located in the right and left inferior parietal gyri (Fig. 3).

Discussion

Previous studies reported white matter abnormalities such as decreased FA and/or increased MD and RD in TSC patients, but only for specific white matter pathways or ROIs. This study extends these findings by providing the first detailed unbiased report of global and regional white matter connectivity as well as whole brain network organization in TSC patients. In addition to traditional atlas-based parcellation approaches, we also used a gyral pattern-based parcellation scheme that allowed us to examine short- and long-range white matter connectivity in the whole brain. Moreover, we performed graph theoretical analysis using the gyral pattern- and atlas-based nodes. We report

Table 5 Spearman correlation between gyral connectivity and corpus callosum connectivity and tuber load

Correlation with tuber load	First	Second	Third	Fourth	Fifth or more	Corpus callosum
FA	−0.086 (0.727)	−0.307 (0.201)	−0.364 (0.126)	−0.355 (0.136)	−0.118 (0.632)	−0.300 (0.212)
MD	0.749 (0.0002*)	0.836 (<0.0001*)	0.829 (<0.0001*)	0.780 (0.0001*)	0.745 (0.0003*)	0.658 (0.002*)
AD	0.742 (0.0003*)	0.748 (0.0002*)	0.757 (0.0002*)	0.782 (0.0001*)	0.847 (<0.0001*)	0.619 (0.005*)
RD	0.621 (0.005*)	0.716 (0.0006*)	0.742 (0.0003*)	0.680 (0.001*)	0.571 (0.011)	0.570 (0.011)
Network density	−0.282 (0.257)	−0.422 (0.082)	−0.539 (0.021)	−0.594 (0.009)	−0.696 (0.001*)	−0.373 (0.128)

Note: data are denoted as correlation coefficient (*P*-value).
*$P < 0.008$.

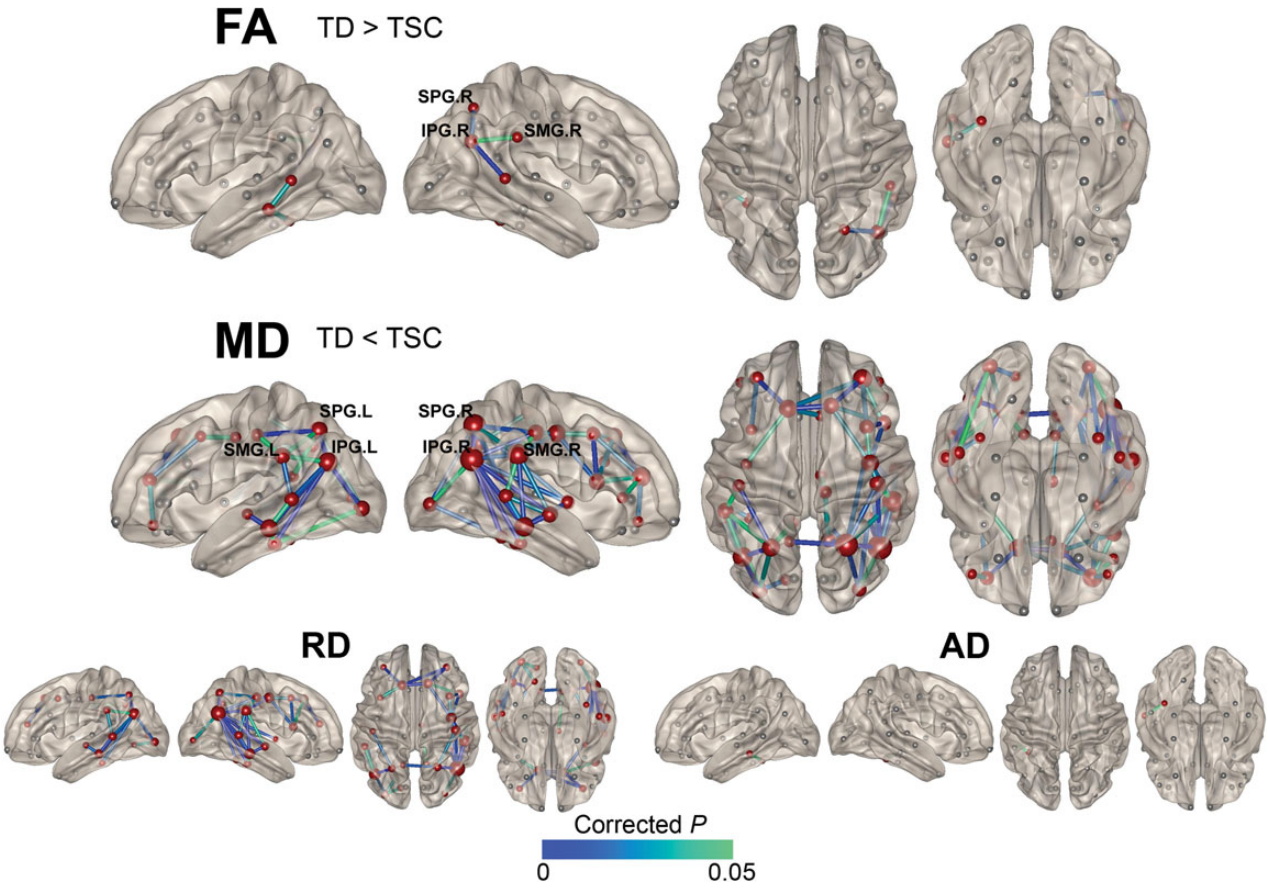

Figure 2. Structural connections showing significantly lower FA and higher MD, RD, and AD in TSC patients compared with TD at the 0.05 level of corrected *P*. The number of statistically significant edges is mapped with a sphere of different sizes. IPG: inferior parietal gyrus; SPG: superior parietal gyrus; SMG: supramarginal gyrus; R: right; L: left.

new findings that in TSC both short- and long-association fibers are affected, and that interhemispheric connectivity appears to be particularly reduced, leading to increased network clustering within hemispheres. Altered structural connectivity in TSC was correlated with qualitative assessments of tuber load. Furthermore, TSC patients with DD compared with without DD showed connectivity changes primarily in intrahemispheric connections. It is unlikely that any of our significant results were biased by the group differences in head motion and fiber tracking.

Primarily Increased RD Throughout the Entire White Matter in TSC

We found significantly increased MD values, primarily influenced by RD, in the TSC compared with the TD group, reproducing the corpus callosum findings of other groups and narrowing the global changes previously reported to the second–fourth gyral connections (Makki et al. 2007; Krishnan et al. 2010; Peters et al. 2012). These findings are consistent with increased MD observed in the normal appearing white matter and in the regions of tubers in TSC patients (Firat et al. 2006). We extended previous findings by showing that a primary increase in RD persists across the entire white matter. However, the microscopic features giving rise to these global structural changes are unclear. Mouse models of demyelination and dysmyelination showed increased RD with little influence on AD (Song et al. 2005). Altered axonal guidance (Meikle et al. 2007; Choi et al. 2008; Nie et al. 2010), balloon cells, large dysplastic neurons, and increased size and number of astrocytes are evident in animal models of TSC (Uhlmann et al. 2004) and may contribute to alterations in RD

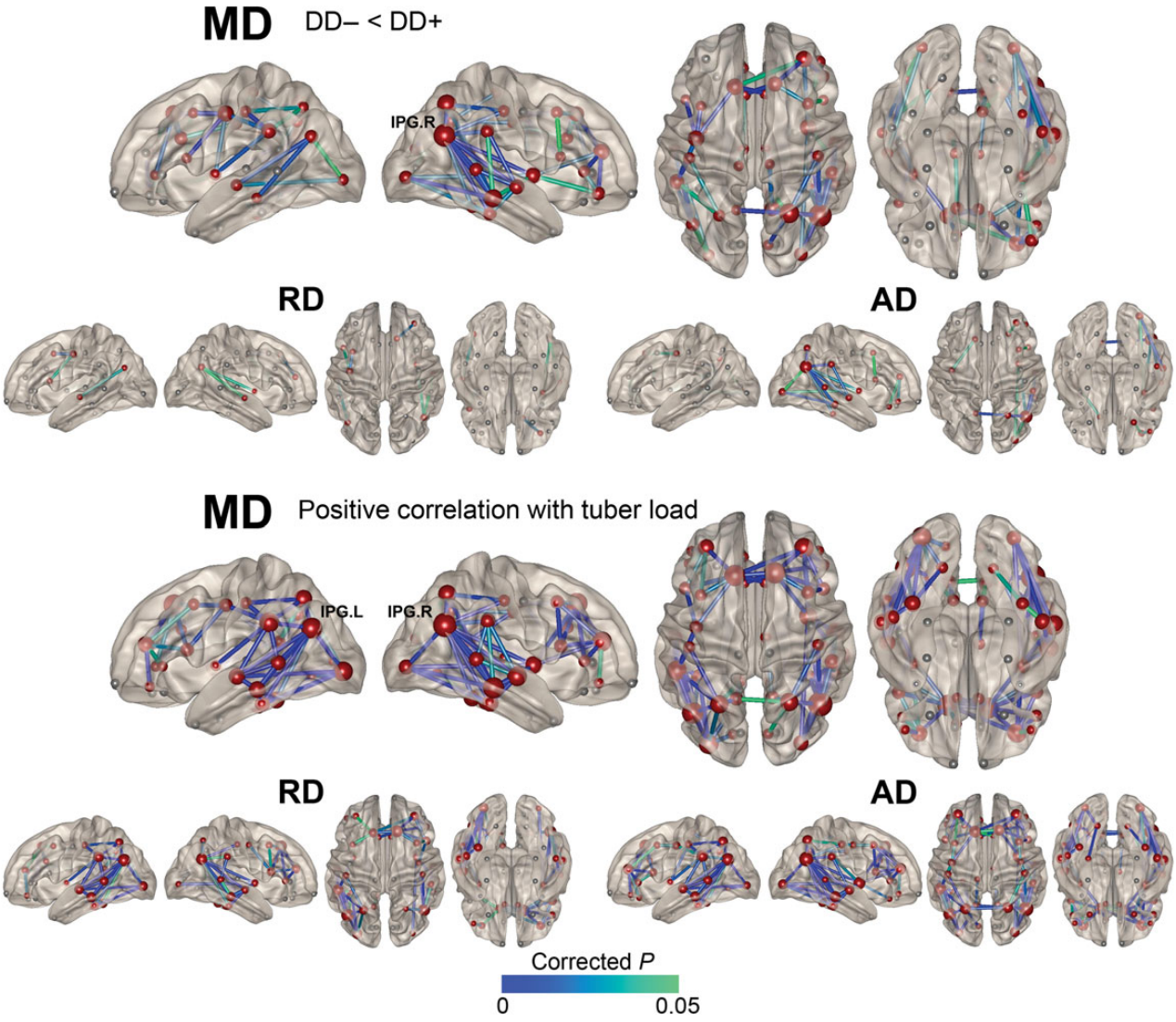

Figure 3. Structural connections showing significantly higher MD, RD, and AD in TSC patients with DD (DD+) compared with those without DD (DD–), and significant positive correlation between MD, RD, and AD and tuber severity in TSC patients at the 0.05 level of corrected *P*. The number of statistically significant edges is mapped with a sphere of different sizes. IPG: inferior parietal gyrus; R: right.

(Makki et al. 2007; Peters et al. 2012). However, unlike prior studies, we did not find a significant FA decrease in TSC for any of the connections due to strict correction for multiple comparisons (Makki et al. 2007; Krishnan et al. 2010; Peters et al. 2012).

Particularly Reduced Interhemispheric Connectivity in TSC

Although altered structural connectivity was observed for most of the connections, the interhemispheric fiber connections were more affected than intrahemispheric fiber connections in TSC compared with TD, showing the highest statistical significance in MD and RD. Furthermore, network density was reduced for corpus callosum in TSC. Interhemispheric network density showed a relatively greater group difference compared with the other gyral connection network densities. This finding indicates decreased strength of coherent white matter connectivity between hemispheres, which in turn impacts global network topology of the TSC brains, resulting in increased network segregation within hemispheres. We performed additional graph theoretical analysis only for connectivity network within the left or right hemispheres. The results did not show significant group differences in the global topology of within-hemisphere networks, which supports the effect of interhemispheric connectivity on the global network. Macroscopic abnormalities in callosal development or agenesis of the corpus callosum can be seen in TSC albeit rarely, and can lead to cognitive impairments (Rosser et al. 2006). The corpus callosum has been suggested to play a role in performance IQ (Alexander et al. 2007), working memory (Takeuchi et al. 2010), complex information processing (Zahr et al. 2009), and language processing (Friederici 2011). Indeed, these are some of the skills that are impaired in various degrees in TSC patients. Microscopic involvement of corpus callosum structure, as detected here, may be associated with TSC cognitive phenotype.

Regional Abnormality of White Matter Connectivity in TSC

We identified 3 regions with the largest number of disrupted connections. The first region was the right inferior parietal gyrus which is reported to play a role in attention (Maruishi et al.

2007) and mental rotation (Gauthier et al. 2002). The second region was the right superior parietal gyrus, which is reported to be activated during working memory tasks (Bell et al. 2006) and is shown to be associated with attentional focalization (Silva-Pereyra et al. 2010). Finally, the third region was the right supramarginal gyrus, which is reported to be important for phonological processing (Hartwigsen et al. 2010) and overcoming emotional egocentricity (Silani et al. 2013). TSC patients show poor performance in the neuropsychological assessments of long-term, verbal, and spatial memory (Ridler et al. 2007), and they have language impairments (Lewis et al. 2013). Such cognitive and behavioral impairments observed in TSC patients might be related to the regional prominence of abnormal white matter connectivity observed here.

Increased AD in addition to RD Primarily for Intrahemispheric Connections in TSC Patients with DD

TSC patients with DD had significantly higher AD, MD, and RD in intrahemispheric connections than those without DD, suggesting that these changes may be driven by a different physiological mechanism than the changes in the corpus callosum. It has been hypothesized that increased AD could result from axonal injury and damage, which cause reduced axonal density or caliber, or axonal loss, and finally increase the extra-axonal space allowing faster water molecule movement parallel to axons (Kumar et al. 2008). However, animal models of TSC do not suggest axonal damage, but instead alterations in axonal guidance (Choi et al. 2008; Nie et al. 2010). Future DTI and pathological studies using animal models of TSC are needed to better understand alterations of RD and AD.

It is interesting to note that TSC patients with DD showed significantly reduced connectivity primarily for the intrahemispheric connections. We suggest that involvement of association fibers within hemispheres may give rise to DD among TSC patients, as these connections support high-level cognitive functions. Patients with DD showed a significant delay in speech and language, in addition to white matter impairments in the bilateral arcuate fasciculus (Gopal et al. 2012). Damage to or dysgenesis of the arcuate fasciculus might be one of the factors causing reduced intrahemispheric connectivity in TSC patients with DD (Lewis et al. 2013). Future studies might benefit from examining intrahemispheric connections in clearly defined groups of children with TSC and/or DD with no other comorbidity to determine if this could be a biomarker for DD and aid in subdividing DD into different phenotypes.

White Matter Connectivity in TSC Patients with ASD and Epilepsy

Although there have been many DTI studies of white matter connectivity of ASD alone (Aoki et al. 2013), there are not many studies comparing the ASD subgroup of TSC patients with those TSC patients without ASD (Peters, Taquet, Prohl, et al. 2013). Lewis et al. (2013) found that TSC patients with ASD had lower FA and higher MD than those without ASD and TD controls in the arcuate fasciculus. Peters et al. (2012) reported significantly decreased FA in the corpus callosum of TSC patients with ASD compared with those without ASD (Peters et al. 2012). Thus, the microstructural integrity of the arcuate fasciculus and corpus callosum is more affected in TSC individuals with ASD. In this study, we also showed decreased FA values for the TSC patients with ASD compared with those without ASD in all the gyral connections as well as the corpus callosum; however, this difference did not reach significance. Moreover, our uncorrected statistical results showed increased MD and RD values in the TSC patients with ASD compared with those without ASD for some of the connections ($P < 0.05$); however, these differences did not reach statistical significance after multiple comparisons correction.

Previous studies have reported white matter abnormalities in TSC patients with epilepsy. Widjaja et al. (2010) found decreased FA for the cortical tubers within the epileptogenic zone compared with the non-epileptogenic zone in patients with epilepsy. Furthermore, same authors reported decreased FA and increased RD in the normal appearing white matter surrounding the cortical tubers. They suggested that these abnormal diffusivity values may reflect cortical dysplasia or could be related to ictal and/or interictal activity. Another study reported increased MD values in tubers compared with the surrounding cortex, and that this increase was especially higher in the epileptogenic tubers (Jansen et al. 2003). These results are in accordance with animal studies where recurrent seizures are shown to cause impairment in myelin development (Dwyer and Wasterlain 1982; Song et al. 2003). However, in this study, we did not find any significant differences between the TSC patients with and without epilepsy. The relatively small sample size for these 2 TSC groups, with increased comorbidity for other disorders (i.e., ASD and DD), and the heterogeneous epileptic regions within each patient might have caused difficulty in the detection of differences between the 2 groups. Further studies need to be performed with a larger sample size to determine if any of the observed trends become significant for the TSC patients with ASD and for those with epilepsy.

Increased Diffusivity Values with Tuber Load Severity in TSC Patients

We explored whether our findings of white matter connectivity are driven by an excess of tubers. Previously, significant correlations between quantitative tuber volume and trace, RD, and FA values were reported for the corpus callosum and the internal capsule, which indicated microstructural changes in the white matter tracts as a result of malformations within the cortical and subcortical tubers (Simao et al. 2010). We found a significant positive correlation between qualitative tuber load and diffusivity values throughout the whole brain, especially in the right and left inferior parietal gyri, in the TSC group. Moreover, we also showed that these results were not affected by fiber tracking. A future study would benefit from a more detailed examination of the tuber count, volume, and location information with white matter connectivity, epilepsy, and cognitive function in TSC.

Methodological Issues

We used gyral segments to define node regions based on their own cortical folding anatomy, which we believe is biologically more meaningful than previous template-based approaches that combine variable numbers of gyri. Specific fiber pathways generally seemed to link and project from a given gyrus to other gyri in prior postmortem and high-resolution imaging studies (Schmahmann and Pandya 2006; Catani et al. 2012). We constructed the connectivity networks based on the FreeSurfer parcellation and analyzed group differences of the graph measures to compare with our approach. Using the Freesurfer parcellation, graph analysis was less sensitive to detecting significant results, which might be due to coarse regional parcellation insufficient for characterizing short-range connectivity. The gyral

node parcellation was also used to effectively categorize and analyze short, neighborhood and long-association fiber connections. This approach becomes particularly useful when dealing with diseased or dysmorphic brains, whose gyral pattern is severely altered and not similar to the normal template (Im et al. 2014).

Conclusions

We provided the first detailed findings on disrupted white matter connectivity and organization in TSC using an unbiased whole-brain approach. Our findings may help better understand the variable clinical phenotypes of TSC and the underlying physiological mechanisms. Future MRI studies with larger sample sizes and neuropsychological testing are needed to better understand the selective effect on white matter connectivity and the neuropsychological consequences.

Supplementary Material

Supplementary material can be found at: http://www.cercor.oxfordjournals.org/.

Funding

This work was supported by Boston Children's Hospital Faculty Career Development Award (K.I.), by National Institutes of Health R01 NS079788 (S.K.W.), and by Boston Children's Hospital Translational Research Program, Autism Speaks, the Tuberous Sclerosis Alliance, Novartis Pharmaceuticals Inc., Hoffman-La Roche, Shire, Department of Defense/ Congressionally Directed Medical Research Program, the Nancy Lurie Marks Foundation and the National Institutes of Health (NIH U01 NS082320 and NIH/NICHD P30 HD018655-31, U54NS092090) (M.S.).

Notes

The authors thank Katyucia Rodrigues for her help with identifying TD participants; Daniel Ginsburg, Rudolph Pienaar, Nicolas Rannou, Chiran Doshi, and Danielle Sliva for their helps with preprocessing of the data. *Conflict of Interest*: None declared.

References

Alexander AL, Lee JE, Lazar M, Boudos R, DuBray MB, Oakes TR, Miller JN, Lu J, Jeong EK, McMahon WM, et al. 2007. Diffusion tensor imaging of the corpus callosum in Autism. Neuroimage. 34:61–73.

Ambi US, Joshi C, Ganeshnavar A, Adarsh E. 2012. Intranasal dexmedetomidine for paediatric sedation for diagnostic magnetic resonance imaging studies. Indian J Anaesth. 56:587–588.

Aoki Y, Abe O, Nippashi Y, Yamasue H. 2013. Comparison of white matter integrity between autism spectrum disorder subjects and typically developing individuals: a meta-analysis of diffusion tensor imaging tractography studies. Mol Autism. 4:25.

APA. 2000. Diagnostic and statistical manual of mental disorders. Arlington (VA): American Psychiatric Association.

Baskin HJ Jr. 2008. The pathogenesis and imaging of the tuberous sclerosis complex. Pediatr Radiol. 38:936–952.

Batalle D, Eixarch E, Figueras F, Munoz-Moreno E, Bargallo N, Illa M, Acosta-Rojas R, Amat-Roldan I, Gratacos E. 2012. Altered small-world topology of structural brain networks in infants with intrauterine growth restriction and its association with later neurodevelopmental outcome. Neuroimage. 60:1352–1366.

Beaulieu C. 2002. The basis of anisotropic water diffusion in the nervous system—a technical review. NMR Biomed. 15:435–455.

Bell EC, Willson MC, Wilman AH, Dave S, Silverstone PH. 2006. Males and females differ in brain activation during cognitive tasks. Neuroimage. 30:529–538.

Bolton PF, Park RJ, Higgins JN, Griffiths PD, Pickles A. 2002. Neuro-epileptic determinants of autism spectrum disorders in tuberous sclerosis complex. Brain. 125:1247–1255.

Catani M, Dell'acqua F, Vergani F, Malik F, Hodge H, Roy P, Valabregue R, Thiebaut de Schotten M. 2012. Short frontal lobe connections of the human brain. Cortex. 48:273–291.

Catani M, Thiebaut de Schotten M. 2008. A diffusion tensor imaging tractography atlas for virtual in vivo dissections. Cortex. 44:1105–1132.

Choi YJ, Di Nardo A, Kramvis I, Meikle L, Kwiatkowski DJ, Sahin M, He X. 2008. Tuberous sclerosis complex proteins control axon formation. Genes Dev. 22:2485–2495.

Chung MK, Robbins SM, Dalton KM, Davidson RJ, Alexander AL, Evans AC. 2005. Cortical thickness analysis in autism with heat kernel smoothing. Neuroimage. 25:1256–1265.

Curatolo P, Bombardieri R, Jozwiak S. 2008. Tuberous sclerosis. Lancet. 372:657–668.

Curatolo P, Verdecchia M, Bombardieri R. 2002. Tuberous sclerosis complex: a review of neurological aspects. Eur J Paediatr Neurol. 6:15–23.

Daducci A, Gerhard S, Griffa A, Lemkaddem A, Cammoun L, Gigandet X, Meuli R, Hagmann P, Thiran JP. 2012. The connectome mapper: an open-source processing pipeline to map connectomes with MRI. PLoS ONE. 7:e48121.

Dale AM, Fischl B, Sereno MI. 1999. Cortical surface-based analysis. I. Segmentation and surface reconstruction. Neuroimage. 9:179–194.

Desikan RS, Segonne F, Fischl B, Quinn BT, Dickerson BC, Blacker D, Buckner RL, Dale AM, Maguire RP, Hyman BT, et al. 2006. An automated labeling system for subdividing the human cerebral cortex on MRI scans into gyral based regions of interest. Neuroimage. 31:968–980.

Dwyer BE, Wasterlain CG. 1982. Electroconvulsive seizures in the immature rat adversely affect myelin accumulation. Exp Neurol. 78:616–628.

Firat AK, Karakas HM, Erdem G, Yakinci C, Bicak U. 2006. Diffusion weighted MR findings of brain involvement in tuberous sclerosis. Diagn Interv Radiol. 12:57–60.

Fischl B, Sereno MI, Dale AM. 1999. Cortical surface-based analysis. II: Inflation, flattening, and a surface-based coordinate system. Neuroimage. 9:195–207.

Fischl B, van der Kouwe A, Destrieux C, Halgren E, Segonne F, Salat DH, Busa E, Seidman LJ, Goldstein J, Kennedy D, et al. 2004. Automatically parcellating the human cerebral cortex. Cereb Cortex. 14:11–22.

Friederici AD. 2011. The brain basis of language processing: from structure to function. Physiol Rev. 91:1357–1392.

Gauthier I, Hayward WG, Tarr MJ, Anderson AW, Skudlarski P, Gore JC. 2002. BOLD activity during mental rotation and viewpoint-dependent object recognition. Neuron. 34:161–171.

Genovese CR, Lazar NA, Nichols T. 2002. Thresholding of statistical maps in functional neuroimaging using the false discovery rate. Neuroimage. 15:870–878.

Gopal SP, Tiwari VN, Veenstra AL, Kumar A, Behen M, Chugani HT, Sundaram SK. 2012. Sensitive diffusion tensor imaging quantification method to identify language pathway abnormalities in children with developmental delay. J Pediatr. 160:147–151.

Hagmann P, Cammoun L, Gigandet X, Meuli R, Honey CJ, Wedeen VJ, Sporns O. 2008. Mapping the structural core of human cerebral cortex. PLoS Biol. 6:e159.

Hagmann P, Sporns O, Madan N, Cammoun L, Pienaar R, Wedeen VJ, Meuli R, Thiran JP, Grant PE. 2010. White matter maturation reshapes structural connectivity in the late developing human brain. Proc Natl Acad Sci USA. 107:19067–19072.

Hartwigsen G, Baumgaertner A, Price CJ, Koehnke M, Ulmer S, Siebner HR. 2010. Phonological decisions require both the left and right supramarginal gyri. Proc Natl Acad Sci USA. 107:16494–16499.

Houenou J, Wessa M, Douaud G, Leboyer M, Chanraud S, Perrin M, Poupon C, Martinot JL, Paillere-Martinot ML. 2007. Increased white matter connectivity in euthymic bipolar patients: diffusion tensor tractography between the subgenual cingulate and the amygdalo-hippocampal complex. Mol Psychiatry. 12:1001–1010.

Im K, Jo HJ, Mangin JF, Evans AC, Kim SI, Lee JM. 2010. Spatial distribution of deep sulcal landmarks and hemispherical asymmetry on the cortical surface. Cereb Cortex. 20:602–611.

Im K, Paldino MJ, Poduri A, Sporns O, Grant PE. 2014. Altered white matter connectivity and network organization in polymicrogyria revealed by individual gyral topology-based analysis. Neuroimage. 86:182–193.

Im K, Pienaar R, Lee JM, Seong JK, Choi YY, Lee KH, Grant PE. 2011. Quantitative comparison and analysis of sulcal patterns using sulcal graph matching: a twin study. Neuroimage. 57:1077–1086.

Im K, Pienaar R, Paldino MJ, Gaab N, Galaburda AM, Grant PE. 2013. Quantification and discrimination of abnormal sulcal patterns in polymicrogyria. Cereb Cortex. 23:3007–3015.

Jansen FE, Braun KP, van Nieuwenhuizen O, Huiskamp G, Vincken KL, van Huffelen AC, van der Grond J. 2003. Diffusion-weighted magnetic resonance imaging and identification of the epileptogenic tuber in patients with tuberous sclerosis. Arch Neurol. 60:1580–1584.

Jenkinson M, Bannister P, Brady M, Smith S. 2002. Improved optimization for the robust and accurate linear registration and motion correction of brain images. Neuroimage. 17:825–841.

Krishnan ML, Commowick O, Jeste SS, Weisenfeld N, Hans A, Gregas MC, Sahin M, Warfield SK. 2010. Diffusion features of white matter in tuberous sclerosis with tractography. Pediatr Neurol. 42:101–106.

Kumar R, Macey PM, Woo MA, Alger JR, Harper RM. 2008. Diffusion tensor imaging demonstrates brainstem and cerebellar abnormalities in congenital central hypoventilation syndrome. Pediatr Res. 64:275–280.

Latora V, Marchiori M. 2001. Efficient behavior of small-world networks. Phys Rev Lett. 87:198701.

Lewis WW, Sahin M, Scherrer B, Peters JM, Suarez RO, Vogel-Farley VK, Jeste SS, Gregas MC, Prabhu SP, Nelson CA III, et al. 2013. Impaired language pathways in tuberous sclerosis complex patients with autism spectrum disorders. Cereb Cortex. 23:1526–1532.

Lo CY, Wang PN, Chou KH, Wang J, He Y, Lin CP. 2010. Diffusion tensor tractography reveals abnormal topological organization in structural cortical networks in Alzheimer's disease. J Neurosci. 30:16876–16885.

Lord C, Risi S, Lambrecht L, Cook EH Jr, Leventhal BL, DiLavore PC, Pickles A, Rutter M. 2000. The autism diagnostic observation schedule-generic: a standard measure of social and communication deficits associated with the spectrum of autism. J Autism Dev Disord. 30:205–223.

Lubisch N, Roskos R, Berkenbosch JW. 2009. Dexmedetomidine for procedural sedation in children with autism and other behavior disorders. Pediatr Neurol. 41:88–94.

Major P, Rakowski S, Simon MV, Cheng ML, Eskandar E, Baron J, Leeman BA, Frosch MP, Thiele EA. 2009. Are cortical tubers epileptogenic? Evidence from electrocorticography. Epilepsia. 50:147–154.

Makki MI, Chugani DC, Janisse J, Chugani HT. 2007. Characteristics of abnormal diffusivity in normal-appearing white matter investigated with diffusion tensor MR imaging in tuberous sclerosis complex. AJNR Am J Neuroradiol. 28:1662–1667.

Maruishi M, Miyatani M, Nakao T, Muranaka H. 2007. Compensatory cortical activation during performance of an attention task by patients with diffuse axonal injury: a functional magnetic resonance imaging study. J Neurol Neurosurg Psychiatry. 78:168–173.

Maslov S, Sneppen K. 2002. Specificity and stability in topology of protein networks. Science. 296:910–913.

Mason KP. 2010. Sedation trends in the 21st century: the transition to dexmedetomidine for radiological imaging studies. Paediatr Anaesth. 20:265–272.

Meikle L, Talos DM, Onda H, Pollizzi K, Rotenberg A, Sahin M, Jensen FE, Kwiatkowski DJ. 2007. A mouse model of tuberous sclerosis: neuronal loss of Tsc1 causes dysplastic and ectopic neurons, reduced myelination, seizure activity, and limited survival. J Neurosci. 27:5546–5558.

Nie D, Di Nardo A, Han JM, Baharanyi H, Kramvis I, Huynh T, Dabora S, Codeluppi S, Pandolfi PP, Pasquale EB, et al. 2010. Tsc2-Rheb signaling regulates EphA-mediated axon guidance. Nat Neurosci. 13:163–172.

Numis AL, Major P, Montenegro MA, Muzykewicz DA, Pulsifer MB, Thiele EA. 2011. Identification of risk factors for autism spectrum disorders in tuberous sclerosis complex. Neurology. 76:981–987.

Onnela JP, Saramaki J, Kertesz J, Kaski K. 2005. Intensity and coherence of motifs in weighted complex networks. Phys Rev E Stat Nonlin Soft Matter Phys. 71:065103.

Peters JM, Sahin M, Vogel-Farley VK, Jeste SS, Nelson CA III, Gregas MC, Prabhu SP, Scherrer B, Warfield SK. 2012. Loss of white matter microstructural integrity is associated with adverse neurological outcome in tuberous sclerosis complex. Acad Radiol. 19:17–25.

Peters JM, Taquet M, Prohl AK, Scherrer B, van Eeghen AM, Prabhu SP, Sahin M, Warfield SK. 2013. Diffusion tensor imaging and related techniques in tuberous sclerosis complex: review and future directions. Future Neurol. 8:583–597.

Peters JM, Taquet M, Vega C, Jeste SS, Fernandez IS, Tan J, Nelson CA III, Sahin M, Warfield SK. 2013. Brain functional networks in syndromic and non-syndromic autism: a graph theoretical study of EEG connectivity. BMC Med. 11:54.

Ridler K, Suckling J, Higgins NJ, de Vries PJ, Stephenson CM, Bolton PF, Bullmore ET. 2007. Neuroanatomical correlates of memory deficits in tuberous sclerosis complex. Cereb Cortex. 17:261–271.

Rosser T, Panigrahy A, McClintock W. 2006. The diverse clinical manifestations of tuberous sclerosis complex: a review. Semin Pediatr Neurol. 13:27–36.

Rubinov M, Sporns O. 2010. Complex network measures of brain connectivity: uses and interpretations. Neuroimage. 52:1059–1069.

Schmahmann JD, Pandya DN. 2006. Fiber pathways of the brain. New York: Oxford University Press.

Shu N, Liu Y, Li K, Duan Y, Wang J, Yu C, Dong H, Ye J, He Y. 2011. Diffusion tensor tractography reveals disrupted topological efficiency in white matter structural networks in multiple sclerosis. Cereb Cortex. 21:2565–2577.

Siddappa R, Riggins J, Kariyanna S, Calkins P, Rotta AT. 2011. High-dose dexmedetomidine sedation for pediatric MRI. Paediatr Anaesth. 21:153–158.

Silani G, Lamm C, Ruff CC, Singer T. 2013. Right supramarginal gyrus is crucial to overcome emotional egocentricity bias in social judgments. J Neurosci. 33:15466–15476.

Silva-Pereyra J, Bernal J, Rodríguez-Camacho M, Yáñez G, Prieto-Corona B, Luviano L, Hernández M, Marosi E, Guerrero V, Rodríguez H. 2010. Poor reading skills may involve a failure to focus attention. Neuroreport. 21:34–38.

Simao G, Raybaud C, Chuang S, Go C, Snead OC, Widjaja E. 2010. Diffusion tensor imaging of commissural and projection white matter in tuberous sclerosis complex and correlation with tuber load. AJNR Am J Neuroradiol. 31:1273–1277.

Song SK, Sun SW, Ju WK, Lin SJ, Cross AH, Neufeld AH. 2003. Diffusion tensor imaging detects and differentiates axon and myelin degeneration in mouse optic nerve after retinal ischemia. Neuroimage. 20:1714–1722.

Song SK, Yoshino J, Le TQ, Lin SJ, Sun SW, Cross AH, Armstrong RC. 2005. Demyelination increases radial diffusivity in corpus callosum of mouse brain. Neuroimage. 26:132–140.

Sporns O, Tononi G, Kotter R. 2005. The human connectome: a structural description of the human brain. PLoS Comput Biol. 1:e42.

Takeuchi H, Sekiguchi A, Taki Y, Yokoyama S, Yomogida Y, Komuro N, Yamanouchi T, Suzuki S, Kawashima R. 2010. Training of working memory impacts structural connectivity. J Neurosci. 30:3297–3303.

Tsai P, Sahin M. 2011. Mechanisms of neurocognitive dysfunction and therapeutic considerations in tuberous sclerosis complex. Curr Opin Neurol. 24:106–113.

Tzourio-Mazoyer N, Landeau B, Papathanassiou D, Crivello F, Etard O, Delcroix N, Mazoyer B, Joliot M. 2002. Automated anatomical labeling of activations in SPM using a macroscopic anatomical parcellation of the MNI MRI single-subject brain. Neuroimage. 15:273–289.

Uhlmann EJ, Li W, Scheidenhelm DK, Gau CL, Tamanoi F, Gutmann DH. 2004. Loss of tuberous sclerosis complex 1 (Tsc1) expression results in increased Rheb/S6K pathway signaling important for astrocyte cell size regulation. Glia. 47:180–188.

van Wijk BC, Stam CJ, Daffertshofer A. 2010. Comparing brain networks of different size and connectivity density using graph theory. PLoS ONE. 5:e13701.

Watts DJ, Strogatz SH. 1998. Collective dynamics of "small-world" networks. Nature. 393:440–442.

Widjaja E, Simao G, Mahmoodabadi SZ, Ochi A, Snead OC, Rutka J, Otsubo H. 2010. Diffusion tensor imaging identifies changes in normal-appearing white matter within the epileptogenic zone in tuberous sclerosis complex. Epilepsy Res. 89:246–253.

Yan C, Gong G, Wang J, Wang D, Liu D, Zhu C, Chen ZJ, Evans A, Zang Y, He Y. 2011. Sex- and brain size-related small-world structural cortical networks in young adults: a DTI tractography study. Cereb Cortex. 21:449–458.

Yendiki A, Koldewyn K, Kakunoori S, Kanwisher N, Fischl B. 2013. Spurious group differences due to head motion in a diffusion MRI study. Neuroimage. 88C:79–90.

Zahr NM, Rohlfing T, Pfefferbaum A, Sullivan EV. 2009. Problem solving, working memory, and motor correlates of association and commissural fiber bundles in normal aging: a quantitative fiber tracking study. Neuroimage. 44:1050–1062.

Zalesky A, Fornito A, Harding IH, Cocchi L, Yucel M, Pantelis C, Bullmore ET. 2010. Whole-brain anatomical networks: does the choice of nodes matter? Neuroimage. 50:970–983.

Zhang Z, Liao W, Chen H, Mantini D, Ding JR, Xu Q, Wang Z, Yuan C, Chen G, Jiao Q, et al. 2011. Altered functional-structural coupling of large-scale brain networks in idiopathic generalized epilepsy. Brain. 134:2912–2928.